Low-Dose Computed Tomography Filtering Using Geodesic Distances

Daniel A. Góes*
Centro Universitário Campo Limpo Paulista - UNIFACCAMP
Programa de Mestrado em Ciência da Computação

Nelson D. A. Mascarenhas
Universidade Federal de São Carlos - UFSCar
Departamento de Computação
Centro Universitário Campo Limpo Paulista - UNIFACCAMP
Programa de Mestrado em Ciência da Computação

***Abstract*—Due to the concerns related to patient exposure to X-ray, the dosage used in computed tomography must be reduced (Low-dose Computed Tomography - LDCT). One of the effects of LDCT is the degradation in the quality of the final reconstructed image. In this work, we propose a method of filtering LDCT sinograms that are subject to signal-dependent Poisson noise. To filter this type of noise, we use a Bayesian approach, changing the Non-local Means (NLM) algorithm to use geodesic stochastic distances for Gamma distribution, the conjugate prior to Poisson, as a similarity metric between each projection point. Among the geodesic distances evaluated, we found a closed solution for the Shannon entropy for Gamma distributions. We compare our method with the following methods based on NLM: Poisson-NLM, Stochastic Poisson NLM, Stochastic Gamma NLM and the original NLM after Anscombe transform. We also compare with BM3D after Anscombe transform. Comparisons are made on the final images reconstructed by the Filtered-Back Projection (FBP) and Projection onto Convex Sets (POCS) methods using the metrics PSNR and SSIM.**

I. Introduction

Computed tomography is a technique that uses ionizing radiation, X-ray being the most common, to generate the scanned object image cuts. Due to the concern with the amount of radiation to which a patient is submitted, [1] and [2], low-dose computed tomography (LDCT) techniques have been developed to utilize the lowest radiation doses possible.

Tomographic projections are corrupted with signal-dependent noise that can be modeled as Poisson noise, [2]. With the reduction in the number of photons, the degradation by noise is accentuated.

Buades et al. (2005) presented a new denoising method, Non-Local Means (NLM), for images corrupted by Gaussian noise using an auto similarity concept.

This work modifies the Non-Local Means using a Bayesian approach to filter Poisson noise. We evaluate our method by filtering sinograms obtained by LDCT, comparing the results with other methods.

II. Noise

The X-ray emitter of a computed tomography scanner emits a poly-energetic beam, [3]. Materials have different attenuation coefficients for each energy band, [4], so the beam incident on a receiver can be described as polychromatic, [5].

*During the development of this work, D. A. Góes was with the Master's Program in Computer Science, UNIFACCAMP

In computed tomography, the noise can be described by a Compound Poisson distribution:

$$Y = \sum_{n=1}^{N} \Phi_n \tag{1}$$

where N represents the number of detected photons, which obeys a Poisson distribution, and Φ_n are random variables, equally distributed, that model the energy of each photon, the probability distribution of Φ_n being derived from the incident spectrum.

Without spectral information of the incident beam, it is not possible to estimate the Compound Poisson distribution. In this work, we consider the model in which the detection process consists of counting the number of incident photons, thus obeying a typical Poisson distribution.

$$Pr(y_i = k|\lambda_i) = \frac{e^{-y_i}\lambda_i^k}{k!} \tag{2}$$

where λ_i is the average rate of photons arriving at the detector i and y_i is the observed photon quantity. $Pr(y_i = k|\lambda_i)$ is the probability of y_i to assume the value k, $k \in \mathbb{Z}^+$, with a photon rate of λ_i.

III. Non-Local Means

Given an input noisy image Y, resulting from degradation of an original, noise-free image X, the Non-Local Means (NLM) method obtains an estimate $\hat{X}$, for the image X, where each pixel $\hat{x}_i$ is calculated by:

$$\hat{x}_i = \frac{1}{w_i} \sum_{j \in B(i,r)} w_{ij} y_j \tag{3}$$

where $0 \leq w_{ij} \leq 1$, $w_i = \sum_{j \in B(i,r)} w_{ij}$, $B(i,r)$ is the search square window of size r, centered on i, and the weights w_{ij} are:

$$w_{ij} = exp(\frac{-1}{\sigma^2}\|y_i - y_j\|_{2,a}^2) \tag{4}$$

σ is a parameter that controls the intensity of the filter, y_i and y_j are vectors representing the similarity window centered on i and j respectively.

IV. Theoretical Foundation

A. Bayesian Approach

Considering an ideal noise-free sinogram X and a given sinogram Y corrupted by Poisson noise, we can obtain an estimator of X through a Bayesian approach.

$$Pr(X|Y) = \frac{Pr(Y|X)Pr(X)}{Pr(Y)} \tag{5}$$

In this model, the likelihood $Pr(Y|X)$ is the noise distribution, and the posterior distribution $Pr(X|Y)$ gives the estimator for the filtered sinogram. Computing this posterior distribution would require the usage of computationally expensive numerical techniques [6] [7]. Instead, we opted to use conjugate prior distributions, a property that if the prior distribution $Pr(X)$ is conjugate to the likelihood distribution $Pr(Y|X)$, then the posterior distribution is of the same type as the prior distribution.

In the case of Poisson likelihood, its conjugate is the Gamma distribution. Thus, if we assume that a neighborhood in the ideal sinogram obeys a Gamma distribution, then the neighborhood in the estimated sinogram will also obey a Gamma distribution. The Gamma distribution also has the very convenient property of being defined on the non-negative real line, assuring non-negative estimators for the rate of the Poisson distribution.

The geodesic distances used will be calculated between the a posteriori Gamma distributions, in the Bayesian model, using the statistical model of the tomographic reconstruction problem under Poisson noise.

1) Parameters Estimation: The posterior hyperparameters $\hat{\alpha}$ and $\hat{\beta}$ can be obtained from the corresponding hyperparameters of the a priori distribution α and β. These prior parameters are estimated from pre-filtering the sinogram with a 3×3 mean filter.

With the method of moments, the parameters are estimated from the mean (μ) and variance (σ^2) calculated in a 3×3 window of the pre-filtered sinogram.

$$\alpha = \frac{\mu^2}{\sigma^2} \tag{6a}$$

$$\beta = \frac{\mu}{\sigma^2} \tag{6b}$$

The posterior parameters are also estimated through the method of moments:

$$\hat{\alpha} = \alpha + \sum_{i=1}^{n} y_i \tag{7a}$$

$$\hat{\beta} = \beta + n \tag{7b}$$

where $\sum_{i=1}^{n} y_i$ is the sum of the projection values in the noisy sinogram window.

B. Geodesic distances

Geodesic distance is the minimum distance between two points passing through a surface. A Riemannian manifold is a generalization of a surface used for calculating these types of distances.

Rao [8] described the parametric space of a probability distribution family as a Riemannian manifold and derived geodesic distances using the Kullback Leiber divergence. These distances could then be used as similarity metrics between two different distributions belonging to the same probability family.

Menéndez et al. [9] proposed a general method for generating geodesic distances for (h,ϕ)-entropies, introduced by Salicru et al. [10]. The parametric space manifold is given by:

$$H_{\phi}^{h} = h\Big[\int_I \phi\big(f_P(x;\theta)\big)dx\Big] \tag{8}$$

where θ is the hyperparameter vector, $f_P(x;\theta)$ the probability density function and I its support range, $(0,\infty)$ for the Gamma distributions.

The geodesic distance is then defined by:

$$d(\theta_a,\theta_b) = \left| \int_{\theta_a}^{\theta_b} \left[\sum_{i=1}^{M}\sum_{j=1}^{M} g_{ij}(\theta) d\theta_i d\theta_j \right]^{\frac{1}{2}} \right| \tag{9}$$

where θ_a and θ_b are the hyperparameter vectors and g_{ij} is the Hessian of H_{ϕ}^{h}.

$$\begin{aligned} g_{ij}(\theta) = \\ & h''\Big[\textstyle\int_I \phi\big(f_P(x;\theta)\big)dx\Big] \int_I \phi'\big(f_P(x;\theta)\big)\frac{\partial f_P(x;\theta)}{\partial\theta_i}dx \\ & \times \textstyle\int_I \phi'\big(f_P(x;\theta)\big)\frac{\partial f_P(x;\theta)}{\partial\theta_j}dx \\ & + h'\Big[\textstyle\int_I \phi\big(f_P(x;\theta)\big)dx\Big] \\ & \times \textstyle\int_I \phi''\big(f_P(x;\theta)\big)\frac{\partial f_P(x;\theta)}{\partial\theta_i}\frac{\partial f_P(x;\theta)}{\partial\theta_j}dx \end{aligned} \tag{10}$$

TABLE I
(h,ϕ)-ENTROPIES AND THEIR RESPECTIVE $h(x)$, $\phi(x)$ FUNCTIONS

(h,ϕ)-entropy	$h(x)$	$\phi(x)$
Arimoto	$(x^s-1)/(s-1)$	$x^{\frac{1}{s}}, s>0, s\neq1$
Havrda-Charvát	x	$(x^s-x)/(s-1), s>0, s\neq1$
Rényi	$log(x)/(s-1)$	$x^s, s>0, s\neq1$
Shannon	x	$-xlog(x)$
Tsallis	$(x-1)/(s-1)$	$x^s, s>0, s\neq1$

This work uses the (h,ϕ)-entropies described in the table I. For the Tsallis entropy, the distances calculated were equivalent to those obtained by the Havrda-Charvát entropy, despite the different values of g_{ij}. Thus, the results are only presented for the Havrda-Charvát entropy.

For the Gamma distribution, it was only possible to find a closed-form solution for the geodesic distance using Shannon's entropy. For the other entropies, it was possible to calculate the terms g_{ij}, so numerical integration was used to calculate the final distance $d(\theta_a,\theta_b)$.

The Shannon geodesic distance for the Gamma distribution is given by:

$$
\begin{aligned}
&d(\theta_1, \theta_2) = \\
&\quad \Big| \big(\beta_1 - 2\alpha_1 \log(\beta_1) - \beta_1 \log(\beta_1) + \log \Gamma(\alpha_1)\big)^{\frac{1}{2}} \\
&\quad - \big(\beta_2 - 2\alpha_2 \log(\beta_2) - \beta_2 \log(\beta_2) + \log \Gamma(\alpha_2)\big)^{\frac{1}{2}} \Big|
\end{aligned} \tag{11}
$$

V. Proposed Geodesic Filtering Method

The proposed Poisson noise reduction filter is based on Evangelista's [11] approach. In our method, the NLM is modified to use geodesic distances between Gamma distributions, where the parameters are estimated for the posterior distribution using the Bayesian approach.

The comparison between similarity windows is made by calculating the geodesic distance between each element, with the final distance being the sum of these distances. The weight w_{ij} from equation 4 is replaced by:

$$
w_{ij} = exp\left(\frac{-\sum_P d(\theta_{i-p}, \theta_{j-p})}{\sigma^2} \right) \tag{12}
$$

where P indexes all elements of the similarity window.

VI. Evaluation

A. Data Set

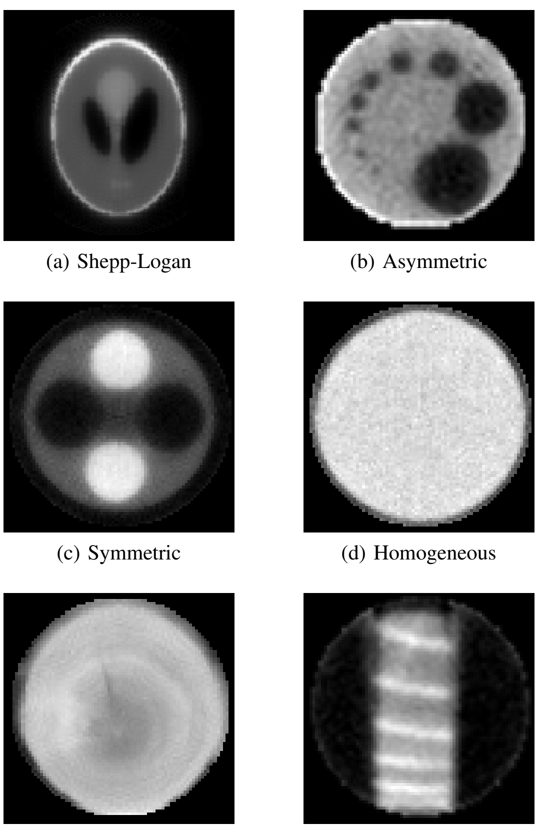

(a) Shepp-Logan (b) Asymmetric

(c) Symmetric (d) Homogeneous

(e) Wood 1 (f) Wood 2

Fig. 1. Noise-Free Reference Images Set Reconstructed by Projection onto Convex Sets (POCS)

The data set used in this work is composed of the Shepp-Logan *phantom* (simulating a cut of the human brain) as well as five real sinograms *phantoms* kindly provided by Prof. Dr. Paulo Estevão Cruvinel from EMBRAPA-CNPDIA [12].

The noisy sinograms were acquired from 3 seconds exposures per projection point, while *phantoms* considered noise-free were acquired from 20 seconds exposures per projection point.

The X-ray energy used was $59.5keV$, the tomographic scanning was performed in an angular rotation of $180°$ with a translation of $1mm$.

The noisy Shepp-Logan sinogram was simulated by calculating the Radon transform of the image, and Poisson noise was introduced in the projections.

The Asymmetric phantom was acquired from a $96mm$ diameter PEXIGLASS® cylinder with ten holes filled with air, with sizes ranging from $0.5mm$ to $5mm$. The projection matrix is 100×100.

The Symmetrical phantom was acquired from a $76mm$ diameter PEXIGLASS® cylinder with four holes, two filled with aluminum and 2 with air. The projection matrix is 80×80.

The Homogeneous phantom was acquired from a $2mm$ thick and $76mm$ of diameter PEXIGLASS® cylinder filled with water. The projection matrix is 80×80.

The Wood 1 phantom was acquired from scanning a $70mm$ diameter *Eucalyptus Saligna* trunk. The projection matrix is 76×76.

The Wood 2 phantom was acquired from a $50mm \times 50mm \times 50mm$ *Pinus Elliottii* trunk. The projection matrix is 62×62.

B. Evaluated Methods

In this work, we evaluate the proposed method using the geodesic distances for the following entropies:

1) Shannon, the comparison is made with the closed-form solution for the distance.
2) Arimoto, the comparison is numeric and with the entropy parameter $s = 1.1$.
3) Havrda-Charvát, the comparison is numeric with the parameter $s = 0.8$.
4) Rényi, the comparison is numeric with the parameter $s = 0.1$.

We compared the proposed method with the original NLM applied in the Anscombe domain (NLM), the Poisson-NLM method [13] (P-NLM), the SP-NLM method [14] (SP-NLM), the stochastic Gamma NLM method [11] (G-NLM), and the BM3D [15] method applied to the Anscombe domain (BM3D).

The Stochastic Poisson NLM (SP-NLM) is an algorithm developed by Bindilatti and Mascarenhas [14] that modifies the NLM by replacing the Euclidean distance with stochastic distances between Poisson distributions. The distances used are Bhattacharyya, Hellinger, Kullback–Leibler, and Rényi. Evangelista [11] proposed an alteration to the SP-NLM, using a Bayesian approach by replacing stochastic distances between Poisson distributions with stochastic distances between Gamma distributions, conjugate of the Poisson. The distances used are Bhattacharyya, Hellinger, Kullback–Leibler, and Rényi.

C. Filtering Parameters

The NLM based methods were evaluated with search windows varying from 5×5 to 11×11. The similarity windows vary from 5×5 up to the size of the search window being used.

Except for Stochastic Poisson NLM, that calculates the σ parameter automatically, in the other methods, the σ parameter varied between 0.1 and 0.5. Except for the homogeneous and Shepp-Logan phantoms that ranged between 0.2 and 0.6.

D. Reconstruction and Evaluation

The sinograms are reconstructed with both FBP and POCS [16] methods. The resulting filtered images are compared with the image obtained by the noise-free sinograms using two similarity metrics, PSN and SSIM [17].

VII. Results

The results presented in tables II through VII are the best ones obtained by each method in each different metric, with the best overall value presented in bold and the second-best in italic. For SP-NLM and G-NLM, only the best performing stochastic distance for each metric is considered. Figure 2 shows some of the filtered Shepp-Logan images.

The standard NLM in the Anscombe domain was not able to achieve comparable results to the other evaluated methods.

The P-NLM method only outperformed the proposed method, in all metrics, in the Symmetric phantom. While in Shepp-Logan and Wood 2, it achieved best results only in one metric each, PSNR in FBP and PSNR in POCS, respectively.

Except for the Homogeneous phantom, the proposed method achieved best results than SP-NLM in virtually all metrics (there was only one with the same result in the Asymmetric phantom).

When comparing our method to the G-NLM, in the Asymmetric phantom, both achieved similar results.

In the Shepp-Logan, our method had best results in the two metrics under FBP, the G-NLM had a best PSNR in POCS, and they had the same result in the last metric. While in the Homogeneous phantom, the G-NLM achieved a superior result in only one metric, PSNR in FBP, with the proposed method having best results in the other three.

For the other three phantoms, Symmetric, Wood 1 and Wood 2, our method outperformed G-NLM in all four metrics.

In comparison to the BM3D, only in the Asymmetric phantom, the BM3D outperformed the proposed method in all metrics. While in the Homogeneous Phantom, our method outperformed BM3D, also in all metrics.

When comparing the PSNR metric with FBP reconstruction, our method achieved best results in five of the tests, having an inferior result only in the Asymmetric phantom.

In the SSIM metric with FBP reconstruction, the BM3D had best results in three phantoms, while our method had a superior result in one phantom, the other two both had the same results.

In POCS reconstruction, both had similar results, with each surpassing the other in half the data set for the PSNR metric, and in SSIM, each method achieved a best result twice and having the same result in two phantoms.

TABLE II
SHEPP-LOGAN RESULTS

Methods	FBP		POCS	
	PSNR (dB)	SSIM	PSNR (dB)	SSIM
Noisy	14.51	0.25	20.22	0.62
Shannon	20.98	0.76	22.11	0.89
Arimoto	21.14	**0.81**	22.14	**0.90**
Havrda Charvát	21.09	0.80	21.68	**0.90**
Rényi	21.07	0.80	21.67	**0.90**
NLM	20.36	0.61	21.86	0.86
P-NLM	**21.20**	0.72	21.77	0.88
SP-NLM	18.84	0.73	18.33	0.86
G-NLM	20.97	0.80	**22.20**	**0.90**
BM3D	21.00	**0.81**	21.30	0.89

TABLE III
ASYMMETRIC RESULTS

Methods	FBP		POCS	
	PSNR (dB)	SSIM	PSNR (dB)	SSIM
Noisy	16.52	0.52	24.27	0.85
Shannon	20.89	0.69	28.85	0.91
Arimoto	21.18	0.70	29.11	0.91
Havrda Charvát	21.24	0.70	29.15	0.91
Rényi	21.16	0.70	29.15	0.91
NLM	20.10	0.67	26.91	0.90
P-NLM	20.81	0.68	28.85	0.90
SP-NLM	20.96	0.69	28.72	0.91
G-NLM	21.26	0.70	29.14	0.91
BM3D	**21.46**	**0.72**	**29.67**	**0.92**

VIII. Conclusion

We developed a method to denoise data corrupted by Poisson noise. We used a Bayesian strategy to alter the Non-Local Means replacing the Euclidean distance by a geodesic statistical distances between a posteriori Gamma distributions. Low-dose computed tomography data were used to evaluate our method.

Due to mathematical simplicity, the proposed method assumes that the original noise-free sinogram obeys a Gamma distribution, since it is the conjugate to the Poisson distribution (used to model the noise). The results obtained show that the approach of using the combined Gamma and Poisson distributions is feasible.

The usage of geodesic distances instead of stochastic ones improved the overall results, obtaining, in general, the best

TABLE IV
SYMMETRIC RESULTS

Methods	FBP PSNR (dB)	FBP SSIM	POCS PSNR (dB)	POCS SSIM
Noisy	20.54	0.45	27.51	0.80
Shannon	27.88	**0.72**	34.42	**0.95**
Arimoto	27.81	**0.72**	33.91	**0.95**
Havrda Charvát	27.70	0.71	34.42	0.94
Rényi	27.77	**0.72**	34.50	**0.95**
NLM	26.27	0.63	33.35	0.93
P-NLM	**28.00**	**0.72**	**34.57**	**0.95**
SP-NLM	25.27	0.67	32.37	0.92
G-NLM	27.81	**0.72**	34.43	**0.95**
BM3D	27.34	**0.72**	33.27	**0.95**

TABLE V
HOMOGENEOUS RESULTS

Methods	FBP PSNR (dB)	FBP SSIM	POCS PSNR (dB)	POCS SSIM
Noisy	13.35	0.12	15.47	0.42
Shannon	18.62	0.32	19.98	0.66
Arimoto	18.92	0.33	20.00	0.66
Havrda Charvát	18.93	0.34	20.82	0.70
Rényi	18.84	0.32	20.69	0.68
NLM	17.35	0.21	18.54	0.57
P-NLM	18.35	0.29	19.56	0.64
SP-NLM	19.26	**0.39**	**23.69**	**0.74**
G-NLM	**19.36**	0.33	20.53	0.69
BM3D	16.53	0.29	19.12	0.66

TABLE VI
WOOD 1 RESULTS

Methods	FBP PSNR (dB)	FBP SSIM	POCS PSNR (dB)	POCS SSIM
Noisy	21.91	0.68	34.08	0.91
Shannon	30.66	0.83	38.48	0.96
Arimoto	29.11	0.84	38.46	**0.97**
Havrda Charvát	**30.69**	0.84	38.12	**0.97**
Rényi	30.64	0.84	38.48	**0.97**
NLM	28.44	0.82	37.75	0.96
P-NLM	28.38	0.81	37.46	0.96
SP-NLM	23.32	0.70	21.38	0.92
G-NLM	30.58	0.83	38.05	0.96
BM3D	29.25	**0.85**	**38.75**	**0.97**

results among the methods based on NLM and close results to BM3D.

Using Shannon's entropy, we were able to find a closed-form geodesic distance for the Gamma distribution. To our knowledge, no previous work has published a similar solution for this model.

TABLE VII
WOOD 2 RESULTS

Methods	FBP PSNR (dB)	FBP SSIM	POCS PSNR (dB)	POCS SSIM
Noisy	19.88	0.56	21.66	0.69
Shannon	26.33	0.68	30.05	0.91
Arimoto	26.21	0.67	30.00	0.91
Havrda Charvát	**26.39**	0.68	30.62	0.91
Rényi	26.23	0.67	30.45	0.90
NLM	24.64	0.68	28.55	0.88
P-NLM	25.76	0.67	30.79	0.91
SP-NLM	18.02	0.47	22.41	0.74
G-NLM	25.35	0.65	29.28	0.89
BM3D	24.80	**0.72**	**31.43**	**0.92**

For the other entropies, in which it was not possible to obtain a closed-form solution for the geodesic distance, numerical integration was used to calculate the final distance, with no perceived loss in the quality of the results when compared to the distance using Shannon's entropy.

It was observed that the quality of the results varies considerably, depending on the value chosen for the σ parameter (equation 12). As future work, there is the possibility of automatically configuring this parameter. Another option is to configure this parameter in an adaptive way, where σ assumes different values for each pixel being filtered.

Using geodesic distances between conjugated distributions to the noise model has the potential to be adapted for other data domains, as synthetic aperture radar images and other forms of medical images like magnetic resonance imaging.

The geodesic distance model proved to be effective when comparing computed tomography sinogram patches. Thus, these distances could be used in the design of descriptors for pattern recognition applications in CT.

This work was published in Digital Signal Processing [18].

The proposed method code was published on the CodeOcean platform at the link:

https://doi.org/10.24433/CO.baa5e6c4-d046-4e20-8eb2-9077c1ce0dee

ACKNOWLEDGMENT

This work was financed in part by the Coordenação de Aperfeiçoamento de Pessoal de Nível Superior - Brasil (CAPES) - Finance Code 001.

We thank Dr. Paulo Estevão Cruvinel of EMBRAPA-CNPDIA who provided the real *phantoms* data used in this work.

The work of N. D. A. Mascarenhas was supported by CNPq, Brazil, through a scholarship under Grant Process 306742/2017-9.

REFERENCES

[1] N. Savage, "Medical imagers lower the dose," *IEEE Spectrum*, vol. 47, no. 3, pp. 14–16, 2010.

[2] J. Z. Liang *et al.*, "Guest editorial low-dose ct: What has been done, and what challenges remain?" *IEEE Transactions on Medical Imaging*, vol. 36, no. 12, pp. 2409–2416, Dec 2017.

[3] I. A. Elbakri and J. A. Fessler, "Efficient and accurate likelihood for iterative image reconstruction in x-ray computed tomography," in *Medical Imaging 2003: Image Processing*, M. Sonka and J. M. Fitzpatrick, Eds., vol. 5032, May 2003, pp. 1839–1850.

[4] L. F. Granato, P. E. Cruvinel, F. Cassaro, and S. Crestana, "A technique for improvement of linear attenuation coefficient maps obtained by means of x-ray tomography in multiple energies," in *Proceedings SIBGRAPI'98. International Symposium on Computer Graphics, Image Processing, and Vision (Cat. No.98EX237)*, Oct 1998, pp. 62–68.

[5] R. Gu and A. Dogandžić, "Blind x-ray ct image reconstruction from polychromatic poisson measurements," *IEEE Transactions on Computational Imaging*, vol. 2, no. 2, pp. 150–165, June 2016.

[6] A. Webb and K. Copsey, *Statistical Pattern Recognition*. Wiley, 2011.

[7] V. Šmídl, V. Smidl, and A. Quinn, *The Variational Bayes Method in Signal Processing*, ser. Signals and Communication Technology. Springer, 2006.

[8] C. R. Rao, "Information and accuracy attainable in the estimation of statistical parameters," *Bulletin of Calcutta Mathematical Society*, vol. 37, no. 3, pp. 81–91, 1945.

[9] M. L. Menéndez, D. Morales, L. Pardo, and M. Salicrú, "(h, Φ)-entropy differential metric," *Applications of Mathematics*, vol. 42, no. 2, pp. 81–98, 1997.

[10] M. Salicrú, M. Menéndez, D. Morales, and L. Pardo, "Asymptotic distribution of (h, ϕ)-entropies," *Communications in Statistics - Theory and Methods*, vol. 22, no. 7, pp. 2015–2031, 1993.

[11] R. C. Evangelista, "Abordagens bayesianas não-locais para filtragem de ruído poisson em imagens tomograficas com baixas taxas de contagem utilizando distâncias estocásticas," Master's thesis, Centro Universitário de Campo Limpo Paulista - UNIFACCAMP, 2017.

[12] R. J. Geraldo, L. M. V. Cura, P. E. Cruvinel, and N. D. A. Mascarenhas, "Low dose CT filtering in the image domain using MAP algorithms," *IEEE Transactions on Radiation and Plasma Medical Sciences*, vol. 1, no. 1, pp. 56–67, 2017.

[13] C. Deledalle, F. Tupin, and L. Denis, "Poisson NL means: Unsupervised non local means for Poisson noise," *Proceeding of the International Conference on Image Processing*, pp. 801 – 804, 2010.

[14] A. A. Bindilatti and N. D. A. Mascarenhas, "A nonlocal Poisson denoising algorithm based on stochastic distances," *IEEE Signal Processing Letters*, vol. 20, no. 11, pp. 1010–1013, Nov 2013.

[15] K. Dabov, A. Foi, V. Katkovnik, and K. Egiazarian, "Image denoising by sparse 3-d transform-domain collaborative filtering," *IEEE Transactions on Image Processing*, vol. 16, no. 8, pp. 2080–2095, 2007.

[16] F. V. Salina and N. D. A. Mascarenhas, "A hybrid estimation theoretic-pocs method for tomographic image reconstruction," in *XVIII Brazilian Symposium on Computer Graphics and Image Processing (SIBGRAPI'05)*, Oct 2005, pp. 220–224.

[17] Z. Wang, A. C. Bovik, H. R. Sheikh, and E. P. Simoncelli, "Image quality assessment: from error visibility to structural similarity," *IEEE Transactions on Image Processing*, vol. 13, no. 4, pp. 600–612, April 2004.

[18] D. A. Góes and N. D. Mascarenhas, "Poisson denoising under a Bayesian nonlocal approach using geodesic distances with low-dose CT applications," *Digital Signal Processing*, vol. 106, p. 102835, Nov 2020.

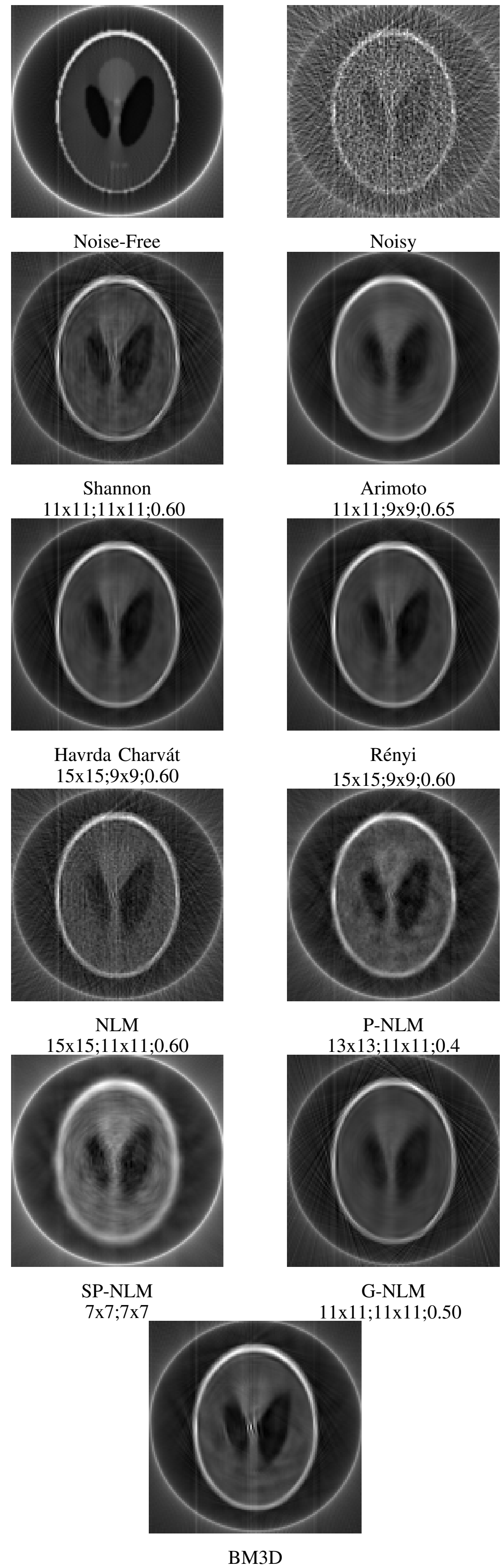

Fig. 2. Images from Shepp-Logan Results for FBP Reconstruction